Journal of Nuclear Materials 395 (2009) 1–10

Contents lists available at ScienceDirect

Journal of Nuclear Materials

journal homepage: www.elsevier.com/locate/jnucmat

Temperature dependence of D removal from JET codeposits by thermo-oxidation

C.K. Tsui [a], A.A. Haasz [a,*], J.W. Davis [a], J.P. Coad [b], A.M. Widdowson [b], J. Likonen [c], A. Hakola [c]

[a] University of Toronto Institute for Aerospace Studies, 4925 Dufferin Street, Toronto, ON, Canada M3H 5T6
[b] Culham Science Centre, EURATOM/UKAEA-Fusion Association, Abingdon, Oxfordshire OX14 3DB, UK
[c] Association EURATOM-TEKES, VTT, P.O. Box 1000, 02044 VTT, Espoo, Finland

ARTICLE INFO

Article history:
Received 1 June 2009
Accepted 18 September 2009

PACS:
28.52.Fa
81.05.Uw
81.65.Mq
82.45.Mp

ABSTRACT

The present study presents new findings for the temperature dependence of D removal from JET Mark II Gas Box divertor codeposits via thermo-oxidation. D removal efficiencies are presented for oxidation with 21 kPa O_2 pressure at temperatures in the range 523–623 K (the 623 K results have been recently published [9,10]). The codeposits analysed in this study have Be concentrations of up to ~40% Be/(Be + C) and thicknesses ranging from 5.5 to 54 μm. The hypothesis that codeposits are porous in nature is supported by post-oxidation surface analysis and codeposit erosion trends. Initial D removal rates from oxidized JET divertor codeposits vary linearly with inherent D content and codeposit thickness, and are independent of Be content and codeposit geometry. The percentage of recoverable D from the JET divertor codeposits was ~65% at 523 K, ~75% at 573 K and ~90% at 623 K, all at 21 kPa. SIMS and NRA surface analyses confirm the fact that codeposit characteristics vary widely even among specimens cut adjacent to one another. This is true even after aggressive oxidation where in some cases the codeposit is totally depleted of the inherent deuterium without a significant reduction in thickness. However, the overall D removal effectiveness of thermo-oxidation appears to be unaffected by these large variations in codeposit structure and composition.

1. Introduction

In the presence of beryllium and carbon plasma-facing components (PFCs), tritium retention in ITER is expected to be dominated by codeposition. During plasma exposure of such PFCs, Be and C atoms and C-containing molecules are released due to physical and chemical sputtering. The released particles are transported in the plasma edge and some are redeposited in conjunction with the hydrogen fuel forming layers of C/Be:H codeposits. Codeposits have been observed not only on surfaces in line of site of the plasma, but also in areas shielded from the plasma. There is no limit to the deposition process. For example, layers of ~250 μm thickness were observed on the inner leg of the JET MKII-GB divertor [1]. In the case of ITER, the specified tritium inventory limit in the torus [2] could be reached after as few as several hundred or as many as several thousand discharges. Once the limit is reached the tritium must be removed from the torus before resuming plasma operation.

One of the proposed T recovery methods from carbon-containing deposits is thermo-oxidation where codeposits are heated and exposed to molecular oxygen; see review [3]. In addition to removing the tritium, the oxidation process also erodes the codeposit itself. Carbon is removed by the formation of CO and CO_2 and tritium is released in the form of water [4,5]. Laboratory produced codeposits tend to be much denser and erode at rates 2–3 orders of magnitude slower than codeposits collected from tokamaks [6]. The rate of codeposit erosion depends on temperature, the partial pressure of oxygen and codeposit structure; in some cases the impurity content of the codeposit also affects the removal rate [7,8].

Recently, thermo-oxidation has been shown to be effective at removing very thick JET codeposits at 623 K and 21 kPa oxygen pressure [9,10]. Approximately 55% of the inherent D in the codeposits was removed after 15 min and >85% was removed after 8 h. In both cases the D removal rates were independent of Be content (0–57% Be/(Be + C)) and codeposit thickness (10–250 μm). Also, D removal from the JET codeposits was found to occur far more rapidly than from thinner tokamak codeposits [7,11]; the initial D release rate was observed to be directly proportional to the inherent D content. These results suggest that the erosion of thick films occurs throughout the entire volume of the codeposit, and not by progressive removal of the front surface [9]. Surface analyses performed after various periods of thermo-oxidation [10] do not show large increases in surface Be concentration following oxidation, nor do they show a progressive erosion from the exposed surface inward, confirming the hypothesis that tokamak codeposits are porous and that oxidation occurs throughout the entire volume of the codeposit.

A next generation reactor such as ITER with codeposits similar to those found in the JET MKII-GB divertor could have ~90%

* Corresponding author. Tel.: +1 416 667 7734; fax: +1 416 667 7799.
E-mail address: tonyhaasz@utias.utoronto.ca (A.A. Haasz).

0022-3115/$ - see front matter © 2009 Elsevier B.V. All rights reserved.
doi:10.1016/j.jnucmat.2009.09.009

reduction in T content by oxidation at 623 K and 21 kPa in about 8 h. The positive results obtained at 623 K raised the question whether oxidation would be viable at lower temperatures. This has led to the objective of the present investigation, namely, to extend our oxidation study to 573 and 523 K.

2. Experiment

2.1. Specimens

Specimens were cut from the Set C tiles that were removed from the JET MKII-GB divertor in 2001 [1]. Specimens were only taken from inboard tiles 1, 3 and 4. Tiles 1 and 3 form the vertical wall of the divertor are within line of sight of the plasma; see Fig. 1. Tile 4 forms the base of the inner divertor and is partially hidden from the plasma by tile 3. These tiles, made of 2D carbon-fibre composites (Dunlop Ltd., concept 1 CFC), were installed in JET during the 3-year 'Gas Box divertor' campaign from 1998 to 2001.

To facilitate comparisons with previous results reported in Refs. [9,10] we use the same notation for specimen identification; see Table 2 in Ref. [9]. For example, specimen 4 (Fig. 1) which is cut from the vertical face of tile 1 is referred to as tile1/sp4. Specimens for the present study were cut in the same poloidal position as those from Refs. [9,10] whenever possible. If insufficient tile surface remained from these poloidal strips, then specimens from adjacent locations were taken. This is the case with tile3/sp5.5 and tile4/sp13 which are adjacent to tile3/sp6 and tile4/sp12.5, respectively. A total of seven specimens were tested, two at 523 K and five at 573 K. Both temperatures were investigated at tile1/spt1 and tile3/sp8, while tile1/sp4, tile3/sp5.5 and tile4/sp13 were only oxidized at 573 K. These specimen locations were selected from the divertor with the goal of obtaining a diverse set of codeposit characteristics including thickness and concentrations of D, Be and C based on pre-oxidation surface analysis [1,9]. Unfortunately, the thickest and most D-rich codeposits located in the shadowed region and up onto the sloping part of tile 4, tile4/sp9 through tile4/sp10, respectively, were consumed in our previous experiments [9,10] and no material remains for further experimentation.

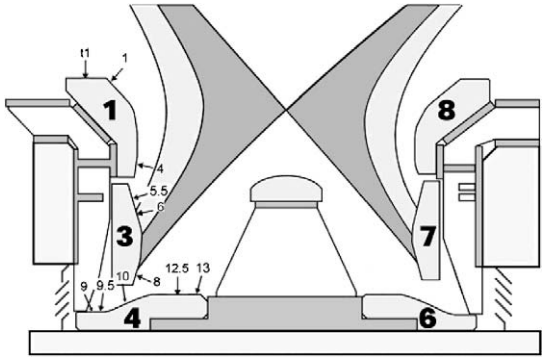

Fig. 1. Schematic of the JET MKII-GB divertor: arrows indicate the locations of the specimens discussed in this study.

2.2. Surface analysis

Details of the surface analysis methods used here are presented in Refs. [1,9,12,13]; here we provide a brief summary. Codeposit tiles were characterized using nuclear reaction analysis (NRA), Rutherford backscattering spectroscopy (RBS), secondary ion mass spectrometry (SIMS), and mechanical micrometer measurements. Deuterium, beryllium and carbon concentrations were obtained from NRA measurements using the reactions $^{2}D(^{3}He, p)^{4}He$, $^{9}Be(^{3}He, p)^{11}B$ and $^{12}C(^{3}He, p)^{14}N$, respectively. Controlled by the penetration depth of the emitted proton, the measurements correspond to the first ~7, ~2 and ~1 μm for D, Be and C, respectively. The reported NRA areal concentrations (per m^2) are restricted to the probing depth and do not account for the entire codeposit thickness. However, assuming a uniform codeposit within the first 7 μm, we can estimate the concentrations within the first micrometer of the surface by dividing the NRA concentrations by these ranges. Table 1 contains the measured NRA values and the scaled (shown as 'adjusted' in the tables) concentrations in the first micrometer for the specimens tested in the present study.

Sputter SIMS was performed using 5 keV O_2^+ to obtain depth profiles of the elemental concentrations in the codeposits. Depth calibration is based on the sputter time and sputter rate, the latter being determined by profilometry measurements. Just before reaching the interface between the substrate and the codeposit the SIMS depth profiling was stopped and the crater depth was measured; typically the D or ^{12}C signals were used for determining the location of the interface. Dividing the crater depth with the sputter time gives the sputter rate. For this study, the sputter rate was determined for specimens tile1/sp4 and tile3/sp8 (after oxidation at 523 K) and the average of these results (~1.5 nm/s) was used for the other specimens. In practice, the accuracy of the profilometry measurements is limited by surfaces roughness, which is

Table 1
Pre-oxidation surface analysis data for specimens used in this study: taken from Refs. [9,10]. The surface analyses were performed in 2004 and 2008, respectively. If an exact poloidal match is not available from Refs. [9,10], data from the closest analysed specimen is reported. Specifically, tile3/sp6 (adjacent to tile3/sp5.5) and tile4/sp12.5 (adjacent to tile4/sp13) were analysed as no material remained from sp5.5 and sp13.

(i) Tile number and specimen location	(ii) Initial codeposit thickness (μm)	NRA: outer layer			NRA: outer layer (adjusted)						
		(iii) 10^{22} D/m^2	(iv) 10^{22} Be/m^2	(v) 10^{22} C/m^2	(vi) Col. (iii)/7 10^{22} D/m^2	(vii) Col. (iv)/2 10^{22} Be/m^2	(viii) Col. (v)/1 10^{22} C/m^2	(ix) D/(Be + C)	(x) Be/(Be + C)	(xi) D/C	(xii) Be/C
tile1/spt1 [9]	n/a	1.7	3.2	6.7	0.24	1.6	6.7	0.03	0.19	0.04	0.24
tile1/spt1 [10]	50	2.0	3.5	5.5	0.28	1.8	5.5	0.04	0.24	0.051	0.32
tile1/sp4 [9]	17	8.2	8.6	3.2	1.2	4.3	3.2	0.16	0.57	0.38	1.34
tile1/sp4 [10]	21	5.7	5.1	3.7	0.81	2.5	3.7	0.13	0.40	0.218	0.68
tile3/sp5.5 [9]	35	14.0	1.9	6.0	2.0	1.0	6.0	0.29	0.14	0.33	0.14
tile3/sp6 [10]	54	11.6	1.8	4.7	1.66	0.9	4.7	0.30	0.16	0.351	0.19
tile3/sp8 [9]	31	7.3	2.1	6.2	1.0	1.0	6.2	0.14	0.14	0.16	0.17
tile3/sp8 [10]	25	15.9	1.9	5.3	2.27	0.9	5.3	0.37	0.15	0.429	0.17
tile4/sp13 [9]	15	9.7	0.8	6.0	1.39	0.4	6.0	0.22	0.06	0.23	0.22
tile4/sp12.5 [10]	6	4.7	0.8	5.1	0.67	0.4	5.1	0.12	0.07	0.131	0.08

~10 μm. The JET codeposits are especially difficult to analyse with SIMS because the films have complex structures; they are far from the ideal lab-produced films. (We note that the ~1.5 nm/s sputter rate obtained for the present study is somewhat smaller than the ~2.3 nm/s rate previously measured [9,10]; the difference could be related to the focusing of the primary beam.)

2.3. Deuterium content measurement

The D contents of the codeposit films were measured by laser induced thermal desorption spectroscopy (TDS) following the procedure outlined in Refs. [9,10]. Small areas of ~1.7 mm in diameter were heated with a 0.5 ms laser pulse at a heat load of ~1 J/mm^2 to desorb all D and ablate the carbon film. A 40 J neodymium-glass laser at 1064 nm was used. The D is released primarily in the form of HD and D_2. The escaping gases leak into the analysis chamber through a partially closed valve where their flow speeds and the total amount released are measured by residual gas analysis using a quadrupole mass spectrometer (QMS). In addition to the primary masses 2, 3 and 4 (containing D) masses 18 and 20 were also monitored to look for the presence of any D_2O and CD_4. The QMS was calibrated in situ using calibrated H_2 and D_2 leak bottles. The QMS sensitivity to HD was taken as the average of the H_2 and D_2 sensitivities. Prior to TDS, the specimen was allowed to cool to room temperature and the chamber pressure was $<10^{-4}$ Pa.

QMS measurements of signals at masses 18 and 20 indicated that typically less than 4% of the D was released as D_2O or CD_4 for the specimens studied here. In addition, the uncertainty in the measurement technique due to variations in the laser spot size and in the leak bottle calibration is estimated to be about ±15%. We note that these sources of uncertainty are generally substantially smaller than the spread in the data due to spatial variation of the codeposits.

For the majority of the specimens, one laser pulse fired at ~1 J/mm^2 would completely desorb all the D and a subsequent shot released only a negligible amount of D. However, for specimens with very high D concentrations the desorbing D during a 1 J/mm^2 laser pulse would increase the pressure in the analysis chamber to above 6×10^{-4} Pa, saturating the QMS and tripping the over-pressure safety relay. In these cases, the laser was fired several times with a gradually increasing intensity keeping the pressure within the QMS detection range. The laser power was increased until it reached 1 J/mm^2 and the laser was fired two or more times until the final pulse was observed to release less than a few percent of the total D released. The surface temperature achieved by laser heating was not measured, but is expected to be in excess of 900 K as heating above this temperature desorbs all D from codeposits [14].

2.4. Thermo-oxidation

Oxygen exposure and laser-TDS were performed in a spherical vacuum chamber; the apparatus diagram is shown in Fig. 2. Specimens of ~2 cm^2 in area and ~0.5 cm thickness were cut from the surface layers of the JET divertor tiles. The back surface of the specimen was clamped to a ceramic heater; a type K thermocouple was inserted into a hole drilled into the side of the specimen to measure its temperature. The above assembly was mounted within the vacuum chamber with the specimen's front surface facing a window to allow for laser access. The chamber was evacuated and baked at 50 K below the test temperature (e.g., baking at 523 K for 573 K oxidation) for ~16 h yielding a background pressure around 10^{-5} Pa. The specimen was then heated to the test temperature ±10 K using the ceramic heater and oxygen was admitted through a metered valve into the chamber and kept constant at ~21 kPa as measured by a capacitance manometer. The

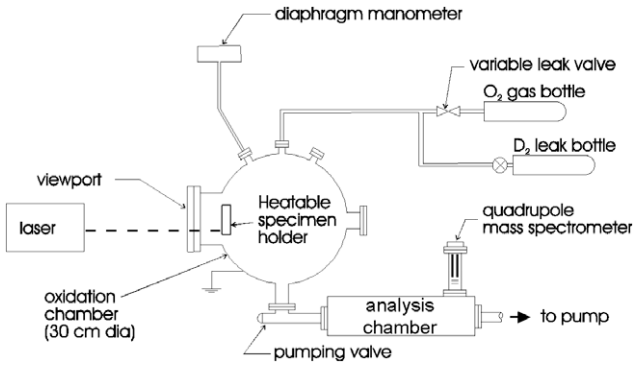

Fig. 2. Schematic diagram of the oxidation apparatus.

specimen was oxidized for a short time step at which point the oxygen was pumped out, the specimen was cooled and the D content measured by laser-TDS. Additional oxidations and D-content measurements were then made to determine the D content as a function of oxidation time; see Figs. 3–5. The shortest time step used was 15 min as limited by the time needed to raise the oxygen pressure to 21 kPa and then evacuate it to below 100 Pa. The amount of tritium released and vented was estimated using an ionization chamber monitoring instrument in the mechanical pump exhaust line; see Table 2. The accuracy of these values was affected by tritium accumulation in the pump oil and backing line, and these values should only be considered order-of-magnitude estimates.

Following oxidation, there was no apparent change in the appearance of any of the specimens used in the present study; similar observations have been noted by others; see review [3] and references therein.

3. Oxidation results and discussion

3.1. D-content measurements

Figs. 3–5 show the D content as a function of oxidation time at 523, 573 and 623 K, respectively, all at 21 kPa oxygen pressure. The specimen D content was measured after system baking at 50 K below the oxidation test temperature with no other heating (data at $t < 0$ in Figs. 3–5) and again after specimen heating in vacuum to

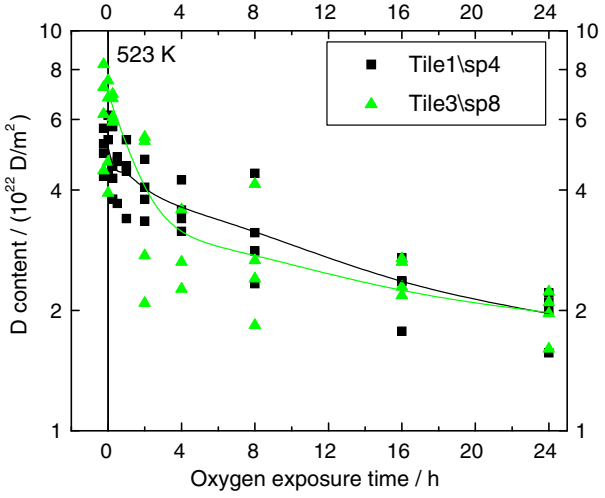

Fig. 3. D content measured by laser-TDS as a function of cumulative oxidation time for specimens oxidized at 523 K.

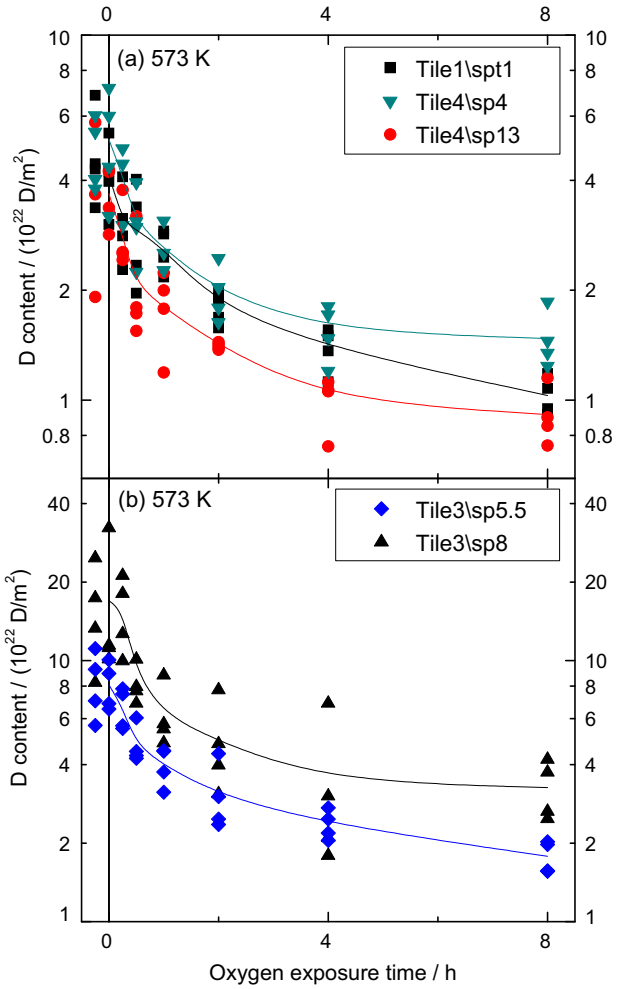

Fig. 4. D content measured by laser-TDS as a function of cumulative oxidation time for specimens oxidized at 573 K; (a) specimens from tiles 1 and 4; (b) specimens from tile 3.

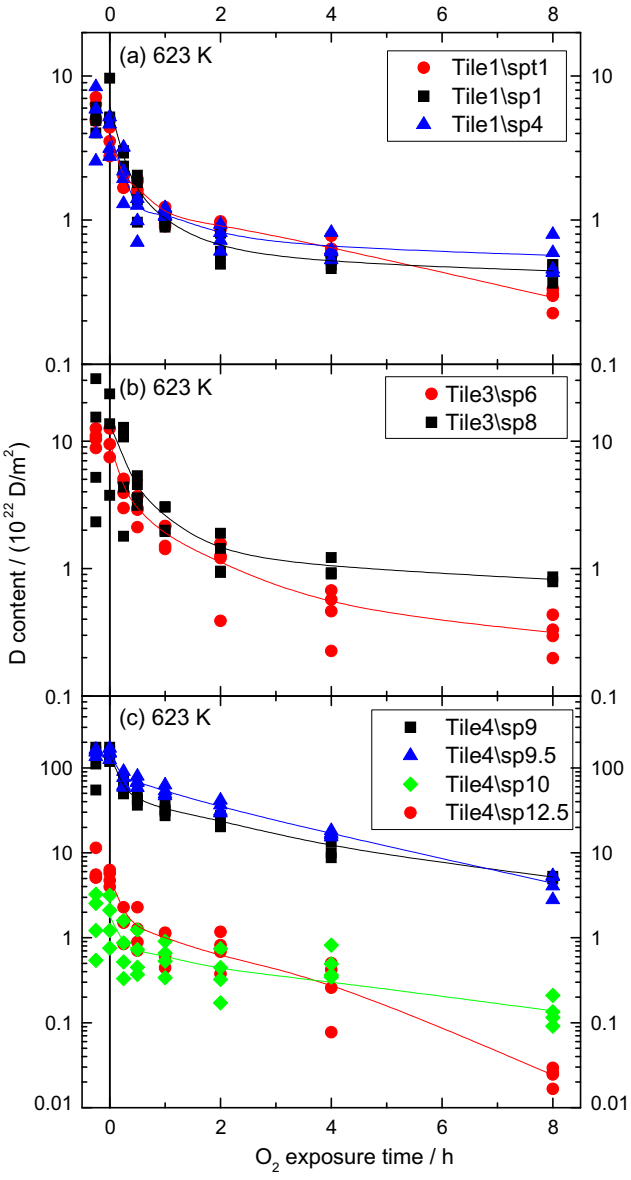

Fig. 5. D content measured by laser-TDS as a function of cumulative oxidation time for specimens oxidized at 623 K; (a) specimens from tiles 1; (b) specimens from tile 3; (c) specimens from tile 4.

the test temperature for 15 min (data $t = 0$ in Figs. 3–5). No significant change in D content within the scatter of the data was observed following heating, which indicates that heating alone does not release trapped D. (We note that due to a power supply malfunction, one specimen (tile4/sp10, see Fig. 5) was heated in vacuum at 723 K for 15 min; however, even after this higher-temperature heating, this specimen also showed a negligible change in D content.) The average value after specimen heating shown at $t = 0$ in Figs. 3–5 shall henceforth be referred to as the 'inherent D content'.

As observed in previous studies [7,8] the initial D removal rate – taken from the slope of the first few sets of data points – indicates that thermo-oxidation is far more effective at higher temperatures. Fig. 6 shows the percentage of the inherent D removed after 15 min of oxidation as a function of temperature. The fraction removed ranges from ~6% at 523 K to ~70% at 623 K. The two heavy dashed lines represent Arrhenius fits for the lower and upper bounds of the data spread. These functions are $3 \times 10^4 \times \exp[-0.6\ \text{eV/kT}]$ for the lower bound and $1.3 \times 10^5 \times \exp[-0.65\ \text{eV/kT}]$ for the upper bound; they give a range of 0.6–0.65 eV for the *effective activation energy* for the complex chemical processes leading to the initial release of D from the bulk of the codeposit.

After prolonged oxidation (8 h at 573 and 623 K and 24 h at 523 K), the D removal rate levels off and the D content approaches a constant such that continued oxidation at the same temperature and pressure will not remove further significant amounts of D; see Figs 3–5. This remaining D after prolonged oxidation shall be referred to as the 'final D content'. Marginal D removal was observed at 523 K with <60% of the inherent D removed after 24 h oxidation; see Fig. 3. The D removal at 573 K is much more effective with ~75% of the inherent D removed after 8 h; see Fig. 4. The highest D removal rate (85–98% removed after 8 h) was observed for oxidation at 623 K [9,10]; see Fig. 5.

3.2. Effects of initial Be content and thickness on D removal

Fig. 7 shows the initial D removal rate (after 15 min of oxidation) at various temperatures and we again note the increase in initial D removal rates at higher temperatures. Data from various other studies [7–10] are also plotted here for comparison. The initial D removal rate is found to be directly proportional to the inherent D content at 573 and 623 K. Insufficient data are available to

Table 2
Laser-TDS D concentrations and T concentrations for JET specimens oxidized at 523, 573 and 623 K.

Oxidation temperature (K)	(i) Tile number and specimen location	(ii) Initial codeposit thickness (μm)	(iii) Inherent D measured by TDS 10^{22} D/m^2	D removed			(vii) T concentration measured in exhaust 10^{17} T/m^2	(viii) T_{meas}/D_{TDS} after 8 h 10^{-6} T/D
				(iv) After 15 min 10^{22} D/m^2	(v) After 8 h 10^{22}D/m^2	(vi) After 24 h 10^{22} D/m^2		
623 [9]	tile1/spt1	–	3.9	2.1	3.6	–	13	33
623 [9]	tile1/sp4	14	3.9	1.8	3.4	–	18	46
623 [9]	tile3/sp6	35	9.8	5.7	9.5	–	6.9	7
623 [9]	tile3/sp8	31	13.6	6.2	12.8	–	–	–
623 [9]	tile4/sp12.5	12	5.2	3.6	5.2	–	18	34
573	tile1/spt1	50	5.2	2.1	4.2	–	22.9	44
573	tile1/sp4	21	4.0	2.3	2.5	–	21.1	53
573	tile3/sp5.5[a]	54[b]	8.1	1.5	6.3	–	26.0	32
573	tile3/sp8	25	16.3	0.8	13	–	27.4	17
573	tile4/sp13[a]	5.5[b]	3.7	0.9	2.8	–	18.6	50
523	tile1/spt1	50	5.3	0.7	2.1	3.3	27.9	53
523	tile3/spt8	25	5.7	−0.7	2.9	3.7	20.5	36

[a] Specimen tile3/sp5.5 is adjacent to tile3/sp6 and tile4/sp13 is adjacent to tile4/sp12.5.
[b] Thickness estimated from measurements taken at the nearest poloidal position.

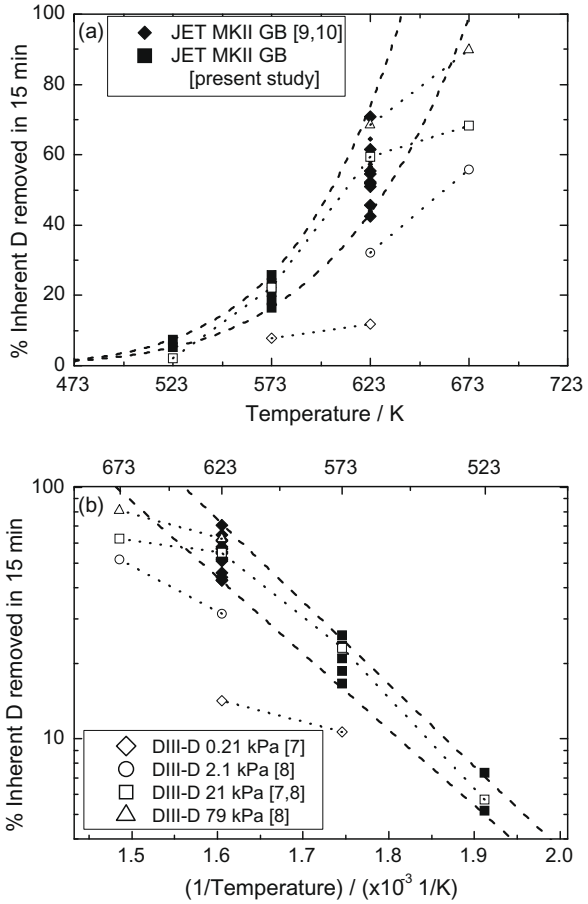

Fig. 6. The fraction of D removed from JET codeposits after 15 min of oxidation at 21 kPa oxygen pressure plotted against (a) temperature, and (b) inverse temperature. The two heavy dashed lines represent Arrhenius fits for the lower and upper bounds of the data spread. These functions are $3 \times 10^4 \times \exp[-0.6\ \text{eV/kT}]$ for the lower and $1.3 \times 10^5 \times \exp[-0.65\ \text{eV/kT}]$ for the upper bound. (Data for oxidation of DIII-D codeposits at 21 kPa are also shown [7,8]; note, however, that for the DIII-D data alone, a slope of ~0.5 eV was reported in Ref. [8].) The legends in (a) and (b) apply to both parts of the figure.

confirm this trend at 523 K, but the data that are available fall on a line that has the same trend as the higher temperature data.

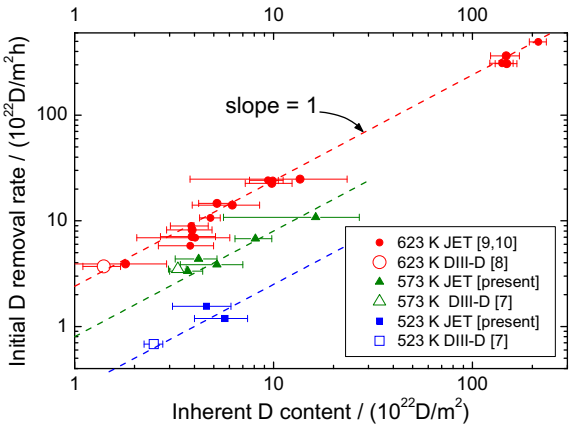

Fig. 7. The amount of D removed in the first 15 min plotted as a function of the inherent D content as measured by laser-TDS. (Data for oxidation of DIII-D codeposits at 21 kPa are also shown [7,8].)

For all specimens at each of the three test temperatures, the same percentage of the inherent D is removed after 15 min of oxidation (Fig. 8) or after the final D content is reached (Fig. 9). (We note that Fig. 9 includes all specimens oxidized at 623 K in Refs. [9,10], some of which do not have corresponding oxidation data at 523 and 573 K in the present study.) This consistency occurs despite large variations in pre-oxidation thickness (5.5–270 μm) and Be concentration (~0–60% Be/(Be + C)). Consistent with this observation, we note in Fig. 9 that after 8 h oxidation at 573 K, the two specimens with the lowest and highest Be content, 6% and 57%, respectively, both show similar – about 70–75% – reductions in D content.

4. Post-oxidation surface analysis

In the discussion below we refer to SIMS profiles in Figs 10–13. In each figure, SIMS profiles are presented for the pre-oxidation *reference* case in part (a) and in parts (b), (c), and (d) for post-oxidation cases at 623, 573, and 523 K, respectively. An O_2 primary beam was used in the SIMS analyses and therefore it was not possible to measure O concentration in the specimens. Surface analyses have revealed that while most codeposits were 'single-layers,' those from the vertical surfaces of tiles 1 and 3 had

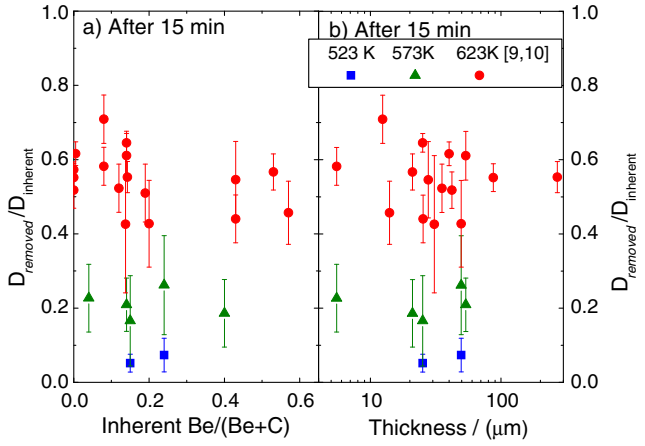

Fig. 8. Fraction of D removed from the JET codeposits after 15 min of oxidation at 523, 573 and 623 K [9]. The data are plotted as a function of (a) pre-oxidation Be content, and (b) codeposit thickness. The fraction of D removed is independent of both Be content and thickness.

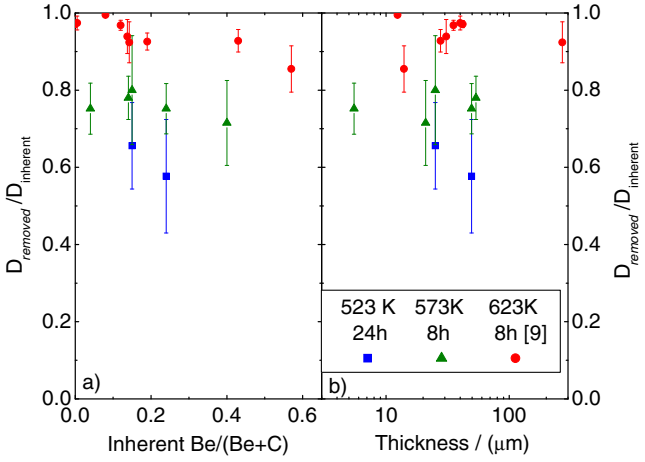

Fig. 9. Fraction of D removed from the JET codeposits after prolonged oxidation (24 h at 523; 8 h at 573 and 623 K [9,10]). The data are plotted as a function of (a) pre-oxidation Be content and (b) codeposit thickness. (*Note:* after 8 h oxidation at 573 K, the two specimens with the lowest and highest Be content, 6% and 57%, respectively, both show similar – about 70–75% – reductions in D content.)

'duplex' structures. The most likely reason for the duplex nature of the codeposit layers is the He-fuelling campaign for one month towards the end of the 1998–2001 Gas Box campaign in 2001 [10,15]. In the discussion that follows, we group the specimens in categories of 'single-layer' and 'duplex structure' according to their structure (measured by SIMS) prior to oxidation. This description is consistent with Ref. [10]. (We note that due to the limited availability of codeposit material, not all specimen locations studied at 623 K in Ref. [10] were oxidized at 573 and 623 K in the present study.) Codeposit thicknesses and NRA concentration data are presented in Table 3.

4.1. Single-layer codeposits

4.1.1. Specimen tile1/spt1 (top of tile 1)

Before oxidation, the specimen was a ~50 μm thick single layer codeposit with Be/C and D/C ratios of ~0.32 and ~0.05, respectively. SIMS profiles of this 'reference' specimen are shown in Fig. 10a.

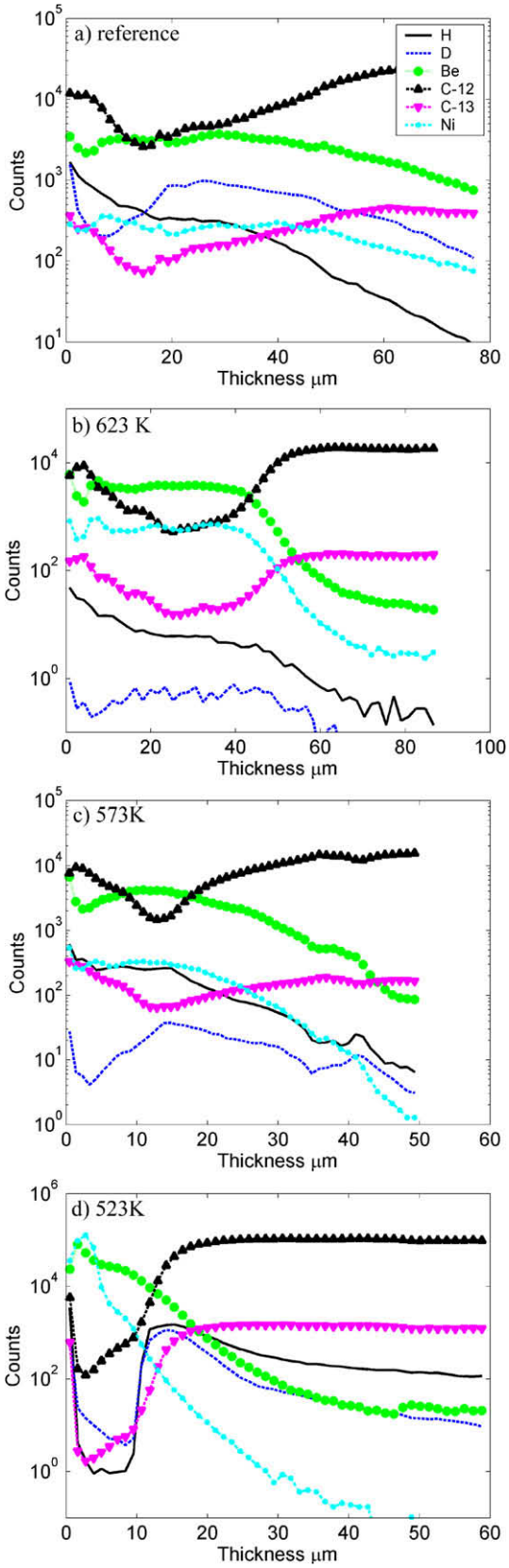

Fig. 10. Sputter SIMS profiles for tile1/spt1 of the (a) reference specimen, (b) after 8 h oxidation at 623 K, (c) after 8 h oxidation at 573 K, and (d) after 24 h oxidation at 523 K. (The legend for the elements applies to all parts of Figs. 10–13.)

After 8 h oxidation at 623 K the thickness and Be/C ratio were unaffected (remaining ~50 μm), but there was some redistribution

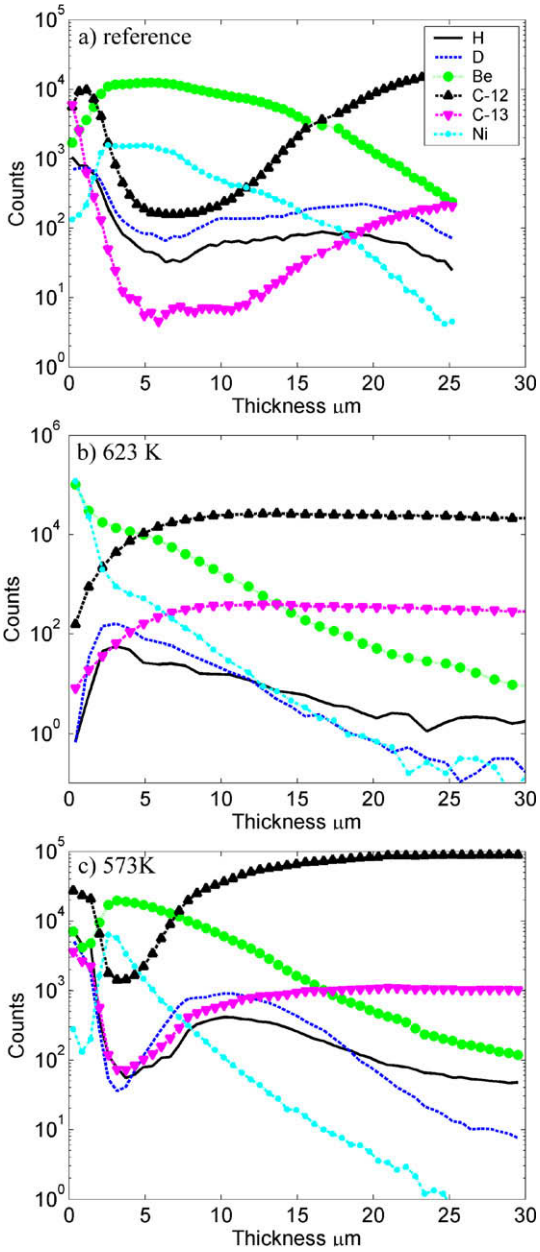

Fig. 11. Sputter SIMS profiles for tile1/sp4 of the (a) reference specimen, (b) after 8 h oxidation at 623 K, and (c) after 8 h oxidation at 573 K.

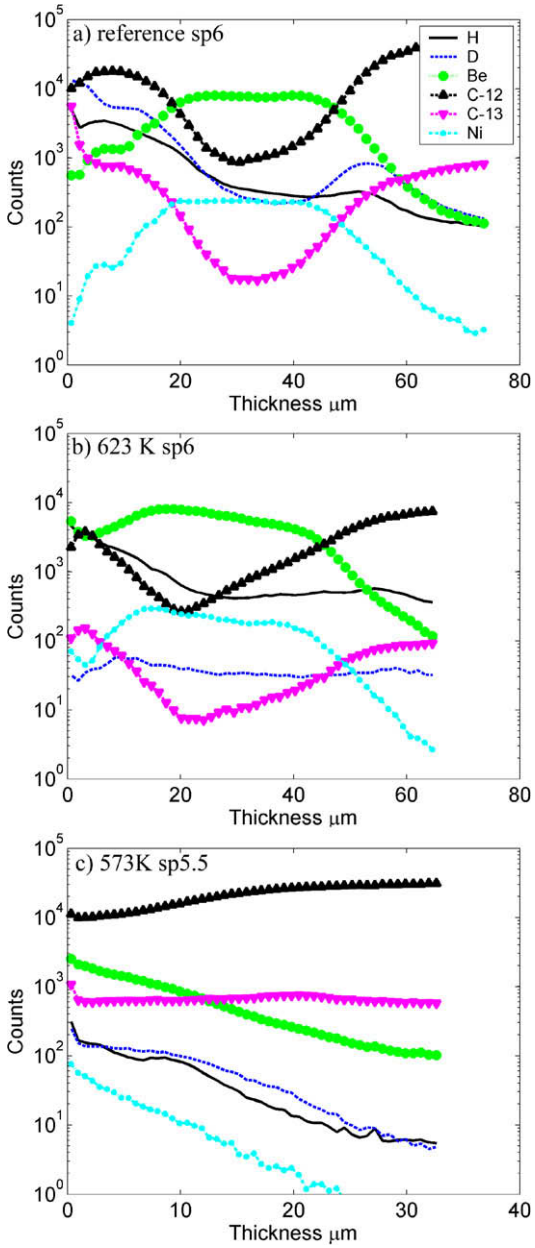

Fig. 12. Sputter SIMS profiles for tile3/sp5.5 and sp6 of the (a) reference specimen, (b) after 8 h oxidation at 623 K, and (c) after 8 h oxidation at 573 K.

of Be and other metals within the film [10]. The D/C ratio was reduced by a factor of 13 with small amounts of D remaining throughout the analysis depth [10].

Oxidation at 573 K also resulted in a redistribution of metals within the film and a significant metal concentration at the depth of 10–20 μm. The Be/C ratio increased by a factor of 3 and the D/C ratio only decreased by a factor of 1.5. The thickness was measured to be 25 μm.

The specimen oxidized for 24 h at 523 K contained much less C in the top 10 μm than the specimen oxidized at 573 K and the reference specimen. RBS measurements show that for the 523 K specimen (*tile1/spt1*) the composition is mainly Be + O (main components: ~20% C, ~30% Be and ~40% O) plus some other metals for 2–5 μm, with some D at or near the surface. We note that oxygen in the reference specimens was most likely introduced during years of air exposure after the tiles have been removed from JET. The films are porous (as our results show for the Be-containing films on tiles 1 and 3), so one would expect the Be to oxidize over time.

The metals show a particularly strong peak in the surface region followed by a strong Be feature in SIMS (see Fig. 10c and d). Not all the surface is quite so clearly layered – another area contains mostly Be + O but also some C according to RBS; here we rely on RBS, as NRA results cannot accurately separate a small C peak from a secondary Be feature. RBS shows that this layer contains mostly Be and O as well as some other metals with some D located very near the surface. Compared to the unoxidized reference material, the D/C ratio decreased by ~10% and the Be/C ratio increased by a factor of 4.5, and the thickness was reduced to ~16 μm. It is not known why the codeposit thickness varies so unexpectedly with oxidation temperature; perhaps the extended oxidation time at 523 K has something to do with it, or perhaps it is simply due to spatial variation

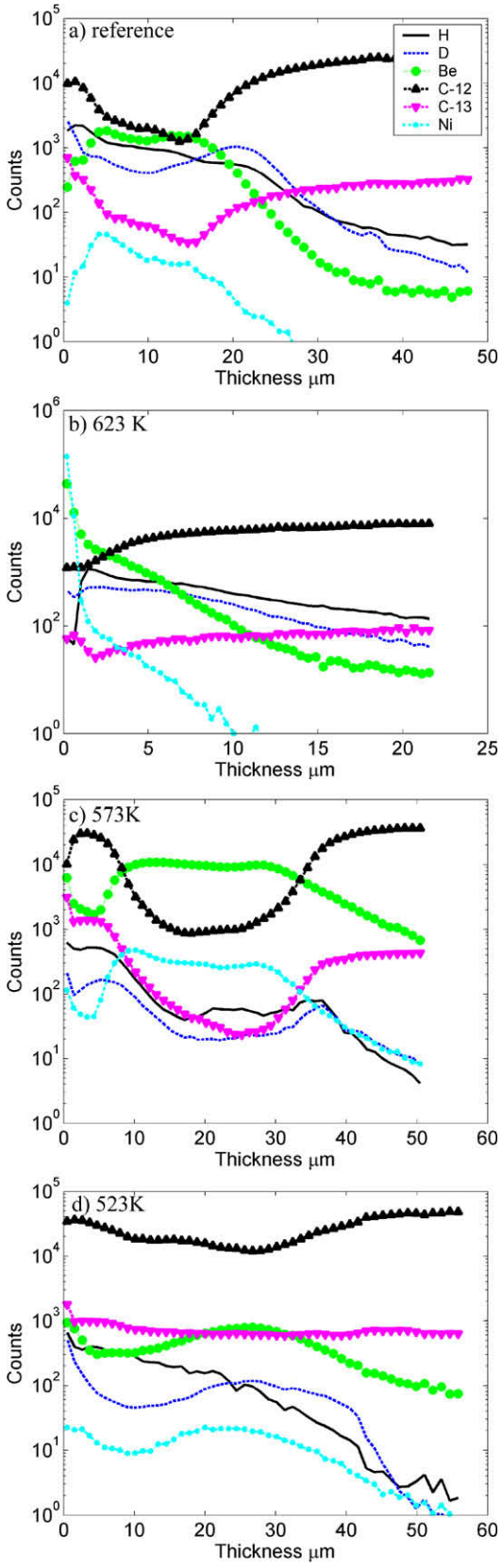

Fig. 13. Sputter SIMS profiles for tile3/sp8 of the (a) reference specimen, (b) after 8 h oxidation at 623 K, (c) after 8 h oxidation at 573 K, and (d) after 24 h oxidation at 523 K.

along the tile. The low D signal in Fig. 10d is due to the much lower sensitivity factor for D in Be compared with D in C.

4.1.2. Specimen tile4/sp12.5 and 13 (upper flat part of tile 4: not exposed to direct plasma, but not shadowed from material re-sputtered from tiles 1 and 3)

This codeposit (spt12.5) was only ~5.5 μm thick with a D/C ratio of ~0.13 and a Be/C ratio of 0.08 [10]. After 8 h oxidation at 623 K, the thickness decreased to ~3.2 μm. The D/C ratio was reduced by a factor of ~30 and the Be/C ratio decreased by a factor of ~2 [10].

After oxidation of a nearby specimen (sp13) for 8 h at 573 K, the D/C ratio was reduced by a factor of 8 and the Be/C ratio decreased by a factor of 2. The thickness was decreased to ~1.5 μm. The decrease in Be/C observed here, and on some other specimens, is attributed to the physical loss of Be, BeO or Be_2C particulates from the surface during oxidation or handling [10]. Unfortunately, tritium contamination of the vacuum system prevented us from measuring the presence of any Be in the vacuum chamber.

We note that no oxidation was performed at 523 K at the tile4/sp12.5(13) location.

4.2. Duplex codeposits

4.2.1. Specimen tile1/sp4 (lower vertical part of tile 1)

Before oxidation, the thickness was ~21 μm. There was a C-rich surface layer while the rest of the film had a high Be/C ~ 0.7 [10]. From RBS and SIMS (Fig. 11a) we see that the C-rich layer contains high amounts of ^{13}C (which may have come from $^{13}CH_4$ puffing) where D/C ~ 1, while the remaining codeposit was dominated by ^{12}C and had a much lower D/C ratio of ~0.2 [10].

After oxidation for 8 h at 623 K, the ^{13}C surface layer was removed and SIMS (Fig. 11b) shows that all that remained was a thin layer of almost pure Be and other metals on top of a few micrometers of more normal codeposit [10]. The D/C fraction was reduced by a factor of 15. NRA suggests that the D removal was not uniform over the surface, with ~10% of the surface retaining some D to >7 μm, perhaps due to the presence of localized particles that resist the scavenging of D by oxygen. The thickness dropped to ~5.4 μm [10].

After oxidation for 8 h at 573 K, we do not see the same peaking of metal impurities and the duplex layer remains; compare Fig. 11b and c. There is a thin layer of C with some D and Be in the outermost micrometer layer. Then a band is seen with almost pure Be and O with some other metals deeper in the codeposit (from 2 to 5 μm by RBS and 2 to 10 μm by SIMS at a different point); see Fig. 11c. Compared to the reference concentrations, the D/C ratio was decreased by a factor of 3.5 and the Be/C ratio was unaffected. The thickness was reduced to 12 μm.

4.2.2. Specimen tile3/sp6 and sp5.5 (upper vertical part of tile 3)

Before oxidation (Fig. 12a), this specimen had a double layer: a Be-rich inner layer and a C- and D-rich outer layer [10]. The overall thickness was ~54 μm. In the outermost micrometer, the D/C ratio was ~1 while it was ~0.35 averaged over the top 7 μm. Significant ^{13}C deposits were found on the very surface; these are likely to have come from the ^{13}C methane puffing experiment [10].

After oxidation for 8 h at 623 K (Fig. 12b), the ^{13}C was lost from the surface, the Be/C ratio was unchanged and the thickness dropped to ~42 μm. The overall two-layer structure was maintained and the D/C ratio was reduced by a factor of ~70 [10].

The tile3/sp5.5 specimen was taken from the poloidal strip adjacent to those of tile3/sp6, and was oxidized at 573 K. There is no sign of the double layered structure. There is some Be, O and D, and ^{13}C at the surface, and then they all tail off uniformly; compare the complete contrast in the SIMS profiles in Fig. 12c with those in Figs. 10d and 11c. After oxidation, the specimen is reduced to 16 μm thickness with an unaffected B/C ratio and a D/C ratio a factor of 10 smaller than the tile3/sp6 reference specimen.

Table 3
NRA data for pre-oxidation (-ref entries) and post-oxidation (-8 h or -24 h entries). Also shown are NRA concentrations 'adjusted' to first micrometer depth according to ion ranges 1, 2, and 7 μm for C, Be, and D, respectively. Specimen notation is the same as in Refs. [9,10].

Tile number	(i) Specimen location, oxidation temperature, and oxidation time	(ii) Codeposit thickness (μm)	NRA: outer layer			NRA: outer layer (adjusted)						
			(iii) 10^{22} D/m^2	(iv) 10^{22} Be/m^2	(v) 10^{22} C/m^2	(vi) Col (iii)/7 10^{22} D/m^2	(vii) Col (iv)/2 10^{22} Be/m^2	(viii) Col (v)/1 10^{22} C/m^2	(ix) D/(Be + C)	(x) Be/(Be + C)	(xi) D/C	(xii) Be/C
1	spt1-ref	50	1.96	3.51	5.47	0.28	1.76	5.47	0.039	0.24	0.051	0.32
1	spt1-623 K-8 h	50	0.14	3.67	5.25	0.02	1.84	5.25	0.003	0.26	0.004	0.35
1	spt1-573 K-8 h	25	0.77	5.78	6.35	0.11	2.89	3.17	0.018	0.48	0.035	0.91
1	spt1-523 K-24 h	16	0.98	8.92	3.08	0.14	4.46	3.08	0.019	0.59	0.045	1.45
1	sp4-ref	21	5.70	5.07	3.73	0.81	2.54	3.73	0.130	0.40	0.218	0.68
1	sp4-623 K-8 h	5.4	0.33	3.95	3.26	0.05	1.98	3.26	0.009	0.38	0.014	0.61
1	sp4-573 K-8 h	12	2.31	7.18	5.41	0.33	3.59	5.41	0.037	0.40	0.061	0.66
3	sp6-ref	54[b]	11.6	1.76	4.73	1.66	0.88	4.73	0.296	0.16	0.351	0.19
3	sp6-623 K-8 h	42	0.16	4.67	4.78	0.02	2.34	4.78	0.003	0.33	0.005	0.49
3	sp5.5[a]-573 K-8 h	16	1.49	2.17	6.63	0.21	1.08	6.63	0.028	0.14	0.032	0.16
3	sp8-ref	25	15.9	1.85	5.29	2.27	0.93	5.29	0.365	0.15	0.429	0.17
3	sp8-623 K-8 h	5.1	0.35	1.27	4.79	0.05	0.63	4.79	0.009	0.12	0.010	0.13
3	sp8-573 K-8 h	37	1.09	4.75	5.93	0.16	2.37	5.93	0.019	0.29	0.026	0.40
3	sp8-523 K-24 h	25	0.93	1.08	8.08	0.13	0.54	8.08	0.015	0.06	0.016	0.07
4	sp12.5-ref	5.5[b]	4.69	0.77	5.10	0.67	0.39	5.10	0.122	0.07	0.131	0.08
4	sp12.5-623 K-8 h	3.2	0.14	0.65	5.27	0.02	0.33	5.27	0.004	0.06	0.004	0.06
4	sp13[a]-573 K-8 h	1.5	0.74	0.60	7.28	0.11	0.30	7.28	0.014	0.04	0.015	0.04

[a] Specimen tile3/sp5.5 is adjacent to tile3/sp6 and tile4/sp13 is adjacent to tile4/sp12.5.
[b] Thickness estimated from measurements taken at the nearest poloidal position.

We note that no oxidation was performed at 523 K at the tile3/sp6(5.5) location.

4.2.3. Specimen tile3/sp8 (lower vertical part of tile 3)

Before oxidation, this specimen had a double layer, though smaller than that observed on tile3/sp6 [10]. Compare Fig. 13a with Fig. 12a. The thickness was ~25 μm, the surface D/C ratio was ~1 and ~0.43 when averaged over the top 7 μm. The Be/C ratio was 0.17 and a trace of ^{13}C was visible on the surface [10].

After oxidation for 8 h at 623 K, all that remained of the original film was a small amount of Be and other metals left on the surface as measured by SIMS (Fig. 13b) and RBS [10]. The D/C ratio was reduced by a factor of ~40 as measured by NRA and the remaining thickness was ~5.1 μm [10].

After oxidation for 8 h at 573 K, the D/C ratio was reduced by a factor of 17. The Be/C ratio is a factor of two above that of the reference. A layer of Be + C (3–4 μm thick) was present at the surface along with a much deeper band rich in Be and Ni, about 10–30 μm from the surface according to SIMS; this Be + C layer was thicker than that observed on tile1/sp4; compare Fig. 13c with Fig. 11c. The thickness was measured to be ~37 μm which is significantly thicker than the 25 μm thick reference specimen.

After oxidation for 24 h at 523 K, only a small amount of Be and a trace of ^{13}C is seen at the surface, then decreasing with depth, with a small D surface peak and some persisting into the surface. SIMS shows that the Be (with some D and metals) increases again, though to a low level in a band about 15 μm from the surface. The post-oxidation thickness was ~25 μm, similar to the reference specimen. The D/C ratio was reduced by a factor of ~27 and the Be/C ratio decreased by a factor of 2.4; see Fig. 13d.

4.3. General observations on surface analysis

There is excellent agreement between the SIMS and IBA results with respect to the composition of the surfaces. There are, however, some minor differences concerning the depth scales; for example, in tile1/sp4 after 573 K oxidation a band of Be is judged to be 2–5 μm from the surface by IBA, whereas in SIMS it appears to be 2–10 μm from the surface. This could be due to varied relative sputtering rates in SIMS, or spatial variations in the codeposit composition since the two analyses were performed on different spots.

^{13}C is detected on the surface of many of the specimens, and this is most likely due to the $^{13}CH_4$ puffing experiment performed on the last days of operation before the shutdown in which the tiles were removed. In some cases such as the tile 3 specimens the ^{13}C is still found on the surface following prolonged oxidation. This is further proof that oxidation does not erode the codeposit from the exposed surface inward. However, the reason why the ^{13}C was not removed by oxidation is unknown, but may be an indication of beryllium carbide formation. We note that the formation of Be_2C for carbon films deposited on Be substrates begins to occur at 550–600 K [16]. This may explain why we observe the removal of the ^{13}C layer during oxidation at 523 K, but not at 573 K.

SIMS and NRA surface analyses confirm the fact that codeposit characteristics vary widely even among specimens cut adjacent to one another. This is true even after aggressive oxidation where in some cases the codeposit is totally depleted of the inherent deuterium without a significant reduction in thickness. In other cases both the thickness and D content are depleted. This irregularity is also noticeable in the scatter of the D-content measurements made by laser desorption. However, these structural variations do not seem to affect the overall D removal effectiveness of thermo-oxidation.

What is the origin of the other metals detected in the codeposits? The JET vessel is made of inconel (basically a nickel–iron–chromium alloy), as are all the tile support structures. Although the confined plasma only interacts with carbon surfaces, charge-exchange neutrals may strike regions that are inconel, and atoms of Ni, Fe, Cr, etc., may be sputtered and transferred to tile surfaces from where some may make it into the plasma. Of the impurities in the plasma, typically 89% are C, 10% are Be, and 1% the metals comprising inconel. Although the largest of these is Ni, the IBA technique, particle induced X-ray emission (PIXE), also detects Fe, Cr and other impurities. Plasma impurities are primarily deposited at the divertor tiles 1 and 3. C may be re-eroded from this region by chemical sputtering, but the Be and metals are not, so the Be:Ni ratio tends to remain roughly constant, whatever the C:Be ratio may be.

5. Conclusion

Initial D removal rates from oxidized JET divertor codeposits vary linearly with inherent D content and codeposit thickness, and are independent of Be content and codeposit geometry. This implies that molecular oxygen is able to deeply penetrate the porous codeposit and that the reaction rate chiefly depends on the oxygen reactivity which increases at higher temperature.

After oxidation, the remaining D in the codeposit represents that trapped in the most energetic a:C–H bonds, possibly in dense localized particles, or isolated by metal oxide impurities. This may imply that the remaining D following prolonged oxidation will continue to be resistant to oxidation following several deposition and oxidation cycles as would occur in a reactor utilizing thermo-oxidation on a regular basis for tritium recovery. However, this must be confirmed in future experiments involving repeated deposition and oxidation cycles. The percentage of recoverable D from the JET divertor codeposits was ~65% at 523 K, ~75% at 573 K and ~90% at 623 K, all at 21 kPa.

SIMS and NRA surface analyses confirm the fact that codeposit characteristics vary widely even among specimens cut adjacent to one another. However, these structural variations do not seem to affect the overall D removal effectiveness of thermo-oxidation.

The measured increase in Be concentration due to the preferential removal of D and C during thermo-oxidation is significantly smaller than expected from the amount of D and C removed as inferred from laser desorption and mass loss measurements, respectively [9]. Some specimens (tile1/sp4, tile3/sp8 and tile4/sp12.5/13) actually show a decrease in Be concentration. This contrasts with DIII-D specimens where boron-to-carbon (B/C) ratios increase as the D is progressively removed during thermo-oxidation [8]. It is suggested that Be is removed from the codeposit during thermo-oxidation through the formation and/or release of BeO or Be_2C particulates.

Implications for ITER: Assuming that the codeposits which will form in the D–T phase in ITER will be similar in impurity content and structure to those observed in the JET MKII-GB divertor, we note that thermo-oxidation at 623 K and 21 kPa can effectively remove >90% of the T in reasonable oxidation times given sufficiently aggressive oxidation conditions. However, thermo-oxidation below 623 K is not expected to be effective for tritium inventory control in ITER.

Acknowledgements

The research performed at the University of Toronto was supported by the Natural Sciences and Engineering Research Council of Canada. We thank Charles Perez for his diligent work in commissioning the experimental facility. The work performed in the EU was conducted under the European Fusion Development Agreement and was partly funded by EURATOM, the UK Engineering and Physical Sciences Research Council, and the National Technology Agency of Finland.

References

[1] J.P. Coad, J. Likonen, M. Rubel, et al., Nucl. Fusion 46 (2006) 350.
[2] ITER Plant Description Document, Safety; Document No. G A0 FDR 1 01-07-13 R1.0, 2001 (Chapter 5).
[3] J.W. Davis, A.A. Haasz, J. Nucl. Mater. 390–391 (2009) 532.
[4] A.A. Haasz, S. Chiu, J.E. Pierre, Y.I. Gudimenko, J. Vac. Sci. Technol. A14 (1996) 184.
[5] S. Alberici, H.K. Hinssen, R. Moormann, C.H. Wu, J. Nucl. Mater. 266–269 (1999) 754.
[6] J.W. Davis, A.A. Haasz, Phys. Scr. T 91 (2001) 33.
[7] R. Ochoukov, A.A. Haasz, J.W. Davis, Phys. Scr. T 124 (2006) 27.
[8] A.A. Haasz, C.K. Tsui, J.W. Davis, R. Ochoukov, Phys. Scr. T 128 (2007) 55.
[9] C.K. Tsui, A.A. Haasz, J.W. Davis, et al., Nucl. Fusion 48 (2008) 035008.
[10] A.A. Haasz, J. Likonen, J.P. Coad, et al., J. Nucl. Mater. 390–391 (2009) 626.
[11] J.W. Davis, A.A. Haasz, J. Nucl. Mater. 266–269 (1999) 478.
[12] J. Likonen, E. Vainonen-Ahlgren, Material Transport and Erosion/Deposition in the JET Torus, JET Fusion Technology Task Force Report on Task JW3-FT-3.10 (Deliverable Nos. 1–4), March 1, 2004.
[13] J.P. Coad, Material Transport and Erosion/Deposition in the JET Torus, JET Fusion Technology Task Force Report on Task JW3-FT-3.10 (Deliverable No. 5), September 3, 2004.
[14] A.A. Haasz, J.W. Davis, J. Nucl. Mater. 232 (1996) 219.
[15] J. Likonen, J.P. Coad, E. Vainonen-Ahlgren, T. Renvall, et al., J. Nucl. Mater. 363–365 (2007) 190–195.
[16] P. Goldstrass, K.U. Klages, Ch. Linsmeier, J. Nucl. Mater. 290–293 (2001) 76.